**Atmospheric
Chemistry
and Physics
Discussions**

This discussion paper is/has been under review for the journal *Atmospheric Chemistry and Physics (ACP)*. Please refer to the corresponding final paper in *ACP* if available.

Cloud condensation nuclei in polluted air and biomass burning smoke near the mega-city Guangzhou, China – Part 1: Size-resolved measurements and implications for the modeling of aerosol particle hygroscopicity and CCN activity

D. Rose[1], A. Nowak[2], P. Achtert[2], A. Wiedensohler[2], M. Hu[3], M. Shao[3], Y. Zhang[3], M. O. Andreae[1], and U. Pöschl[1]

[1]Biogeochemistry Department, Max Planck Institute for Chemistry, Mainz, Germany
[2]Leibniz Institute for Tropospheric Research, Leipzig, Germany

---

CCN in polluted air and biomass burning smoke

D. Rose et al.

Title Page

Abstract	Introduction
Conclusions	References
Tables	Figures

| ◄◄ | ►► |
| ◄ | ► |

| Back | Close |

Full Screen / Esc

Printer-friendly Version

Interactive Discussion

[3]State Key Joint Laboratory of Environmental Simulation and Pollution Control, College of Environmental Sciences and Engineering, Peking University, Beijing, China

Correspondence to: D. Rose (rose@mpch-mainz.mpg.de)

Title Page

Abstract | Introduction

Conclusions | References

Tables | Figures

|◀ | ▶|

◀ | ▶

Back | Close

Full Screen / Esc

Printer-friendly Version

Interactive Discussion

Abstract

Atmospheric aerosol particles serving as cloud condensation nuclei (CCN) are key elements of the hydrological cycle and climate, but their abundance, properties and sources are highly variable and not well known. We have measured and characterized CCN in polluted air and biomass burning smoke during the PRIDE-PRD2006 campaign on 1–30 July 2006 at a rural site ~60 km northwest of the mega-city Guangzhou in southeastern China.

CCN efficiency spectra (activated fraction vs. dry particle diameter; 20–300 nm) were recorded at water vapor supersaturations (S) in the range of 0.07% to 1.27%. Depending on S, the dry CCN activation diameters were in the range of 30–200 nm, corresponding to effective hygroscopicity parameters κ in the range of 0.1–0.5. The hygroscopicity of particles in the accumulation size range was generally higher than that of particles in the nucleation and Aitken size range. The campaign average value of κ for all aerosol particles across the investigated size range was 0.3, which equals the average value of κ for other continental locations. During a strong local biomass burning event, the activation diameters increased by ~10% and the average value of κ dropped to 0.2, which can be considered as characteristic for freshly emitted smoke from the burning of agricultural waste. At low S (≤0.27%), the maximum activated fraction remained generally well below one, which indicates substantial proportions of externally mixed CCN-inactive particles with much lower hygroscopicity – most likely soot particles (up to ~60% at ~250 nm).

The mean CCN number concentrations ($N_{CCN,S}$) ranged from 1100 cm^{-3} at S=0.07% to 16 000 cm^{-3} at S=1.27%, representing ~7% to ~85% of the total aerosol particle number concentration. Based on the measurement data, we have tested different model approaches (power laws and κ-Köhler model) for the approximation/prediction of $N_{CCN,S}$ as a function of water vapor supersaturation, aerosol particle number concentration, size distribution and hygroscopicity. Depending on S and on the model approach, the relative deviations between measured and predicted $N_{CCN,S}$

ranged from a few percent to several hundred percent. The largest deviations occurred at low S and with power laws based on particle number concentration. With the κ-Köhler model and a constant hygroscopicity parameter of 0.3, the deviations were on average less than ∼20%, which confirms that κ=0.3 may be suitable for approximating the hygroscopicity and CCN activity of continental aerosols in large scale models of the atmosphere and climate. On the other hand, the temporal variations of $N_{CCN,S}$ observed during the biomass burning event and in diurnal cycles could not be captured with constant κ (deviations up to ∼80%). With variable κ values obtained from individual CCN efficiency spectra, the relative deviations were on average less than ∼10% and hardly exceeded 20%, confirming the applicability of the κ-Köhler model approach for efficient description of the CCN activity of atmospheric aerosols. Note, however, that different types of κ-parameters have to be distinguished for external mixtures of CCN-active and -inactive aerosol particles.

1 Introduction

Atmospheric aerosol particles that enable the condensation of water vapor and formation of cloud droplets are called cloud condensation nuclei (CCN). Elevated concentrations of CCN tend to increase the concentration and decrease the size of droplets in a cloud. Besides changing the optical properties and radiative effects of clouds on climate, this may lead to the suppression of precipitation in shallow and short-lived clouds but also to greater convective overturning and more precipitation in deep convective clouds (Rosenfeld et al., 2008). The response of cloud characteristics and precipitation processes to increasing anthropogenic aerosol concentrations represents one of the largest uncertainties in the current understanding of climate change. One of the crucial underlying challenges is to determine the ability of aerosol particles to act as CCN under relevant atmospheric conditions, an issue that has received increasing attention over the past years (McFiggans et al., 2006; IAPSAG, 2007; IPCC, 2007; Andreae and Rosenfeld, 2008, and references therein).

In order to incorporate the effects of CCN in meteorological models at all scales, from large eddy simulation (LES) to global climate models (GCM), knowledge of the spatial and temporal distribution of CCN in the atmosphere is essential (Huang et al., 2007). In recent years, anthropogenic emissions of aerosol particles and precursors from Asia have increased significantly (Streets et al., 2000, 2008; Richter et al., 2005; Shao et al., 2006), and numerous studies indicate that anthropogenic aerosol particles have changed cloud microphysical and radiative properties (Xu, 2001; Liu et al., 2004; Massie et al., 2004; Zhang et al., 2004; Wang et al., 2005; Qian et al., 2006; Zhao et al., 2006; Li et al., 2007; Rosenfeld et al., 2007; Deng et al., 2008). Thus, CCN data are required for assessing the impact of anthropogenic aerosol on regional and global climate, but only few CCN measurements have been performed in Asia and in the vicinity of mega-cities and city-clusters which are major source regions of air particulate matter (e.g. Matsumoto et al., 1997; Yum et al., 2005, 2007; Kuwata et al., 2007, 2008).

The Pearl River Delta (PRD) in southeastern China is one of the main centers of economic activity and growth in Asia. Due to strong anthropogenic emissions, the PRD region is often plagued with high aerosol concentrations that lead to not only low visibility, but can also impact the regional radiative balance, precipitation patterns and hydrological cycles (Hagler et al., 2006; Andreae et al., 2008; Fan et al., 2008; Wendisch et al., 2008; Zhang et al., 2008).

Within the "Program of Regional Integrated Experiments of Air Quality over the Pearl River Delta" intensive campaign in July 2006 (PRIDE-PRD2006), we have measured and characterized the CCN properties of aerosol particles in polluted air and biomass burning smoke near the mega-city Guangzhou as a function of particle diameter (30–300 nm) and water vapor supersaturation (0.07–1.27%). In this manuscript, we focus on the results of the size-resolved CCN measurements and on the implications for different approaches of approximating and predicting CCN number concentrations. A follow-up study will address the relations between aerosol chemical composition and CCN activity (Rose et al., 2008a).

CCN in polluted air and biomass burning smoke

D. Rose et al.

2   Methods

2.1   Measurement location, meteorological conditions and supporting data

The measurements were performed over the period of 1–30 July 2006 in Backgarden (23.548056° N, 113.066389° E), a small village ~60 km northwest of Guangzhou on the outskirts of the densely populated center of the PRD. Due to the prevailing southeast monsoon circulation at this time of year, the air masses came mainly from the south/southeast, making this site a rural receptor site for the regional pollution resulting from the outflow of the city cluster around Guangzhou. The average meteorological conditions (arithmetic mean±standard deviation) for the campaign were: 28.9±3.2°C ambient temperature, 78.0±13.7% ambient relative humidity (RH), 997±4 hPa ambient pressure, 1.8±1.2 m s^{-1} local wind speed, 143±53° local wind direction. For more information about the measurement location and meteorological conditions see Garland et al. (2008b).

A two-story building was used exclusively to house the measurement campaign, with most of the instruments placed in air conditioned rooms on the top floor and sample inlets mounted on the rooftop. The main aerosol inlet used in this study was equipped with a Rupprecht & Patashnick PM$_{10}$ inlet (flow rate 16.7 L min^{-1}). The sample flow passed through stainless steel tubing (1.9 cm i.d., 5.1 m length) and a diffusion dryer with silica gel/molecular sieve cartridges (alternating regeneration with dry pressurized air, regeneration cycles 15–50 min, average RH=33±7%). After drying, the sample flow was split into separate lines. One led to the CCN measurement setup described below (0.9 cm i.d. stainless steel, ~4 m length, flow rate 1.5 L min^{-1}); another one was used for aerosol particle size distribution measurements (3–900 nm) with a Twin Differential Mobility Particle Sizer (TDMPS). The inlet, dryer and size distribution measurements were operated by the Leibniz Institute for Tropospheric Research (IfT).

Besides aerosol particle size distribution and CCN activity, on which we focus in this manuscript, a wide range of other aerosol, gas phase, and meteorological parameters were measured to characterize local and regional air pollution (Garland et al., 2008b;

Hua et al., 2008a; Liu et al., 2008). These will be used in a follow-up study addressing the relations between aerosol chemical composition and CCN activity (Rose et al., 2008a).

2.2 CCN measurement and data analysis

2.2.1 Instrumentation and measurement procedure

Size-resolved CCN efficiency spectra (CCN activation curves) were measured with a Droplet Measurement Technologies continuous flow CCN counter (Roberts and Nenes, 2005; Lance et al., 2006) coupled to a Differential Mobility Analyzer (DMA; TSI 3071) and a condensation particle counter (CPC; TSI 3762; Frank et al., 2006; Rose et al., 2008b).

The CCN counter (CCNC) was operated at a total flow rate of $0.5\,L\,min^{-1}$ with a sheath-to-aerosol flow ratio of 10. For the campaign, the average sampling pressure and temperature as measured inside the CCNC were $(1006\pm6)\,hPa$ and $(23.7\pm1.4)°C$, respectively. The effective water vapor supersaturation (S) was regulated by the temperature difference between the upper and lower end of the CCNC flow column (ΔT) and calibrated as described below and in Rose et al. (2008b).

For each CCN measurement cycle, ΔT was set to 5 different levels in the range of 1.98–16.9 K corresponding to S values of 0.068% to 1.27%. For each ΔT and S, respectively, the diameter of the dry aerosol particles selected by the DMA (D) was set to 9 different values in the range of 20–290 nm. At each D, the number concentration of total aerosol particles (condensation nuclei, CN), N_{CN}, was measured with the CPC, and the number concentration of CCN, N_{CCN}, was measured with the CCNC. The integration time for each measurement data point was 50 s, the recording of a CCN efficiency spectrum (N_{CCN}/N_{CN} vs. D) took ~16 min, and the completion of a full measurement cycle comprising CCN efficiency spectra at 5 different supersaturation levels took ~85 min (including 5 min for adjustment between the highest and lowest level of S). Note that for the lowest supersaturation level applied in the atmospheric

measurements, the mean value of $S=0.068\%$ was used for the calculations outlined below, but for simplicity a value of 0.07% is listed in figures and tables.

2.2.2 Calibration of CCN counter

With respect to the effective water vapor supersaturation S, the CCNC was calibrated with ammonium sulfate aerosol as described by Rose et al. (2008b). During the campaign, five calibration experiments were performed, and in each of these experiments multiple CCN efficiency spectra were recorded for 5 different ΔT values. The midpoint activation diameter of each CCN efficiency spectrum was taken as the critical dry diameter for the CCN activation of ammonium sulfate particles, and the corresponding critical supersaturation was calculated with an activity parameterization Köhler model (AP3; Rose et al., 2008b) that can be regarded as the most accurate reference available. Note that other frequently used Köhler models and the corresponding calibration lines would deviate by up to 20% or more, and care has to be taken when comparing the results of different CCN measurement and model studies (Rose et al., 2008). The calculated critical supersaturation was taken as the effective supersaturation at the given ΔT value.

Figure 1 shows the average CCN efficiency spectra obtained from the 5 calibration experiments with ammonium sulfate aerosol, and the corresponding average calibration parameters are given in Table 1. A linear least-squares fit to the data pairs of S and ΔT was taken as the CCNC calibration line for the entire campaign: $S=k_s\Delta T+S_0$ with $k_s=0.08041\%$ K^{-1} and $S_0=-0.09109\%$, $R^2=0.9929$. It was applied to calculate S from the average value of ΔT recorded during each measurement of a CCN efficiency spectrum of atmospheric aerosol. As detailed by Rose et al. (2008b) variations in S are mostly due to variations of the CCNC inlet temperature. The standard deviations of the calibration data points and their maximum deviations from the calibration line ($\Delta S/S$) as listed in Table 1 indicate a relative uncertainty of less than $\sim$7% for S in the CCN measurements reported in this study.

CCN in polluted air and biomass burning smoke

D. Rose et al.

Title Page

Abstract | Introduction

Conclusions | References

Tables | Figures

◀ | ▶

◀ | ▶

Back | Close

Full Screen / Esc

Printer-friendly Version

Interactive Discussion

2.2.3 Correction of measured CCN efficiency spectra

The measured atmospheric CCN efficiency spectra were corrected for multiply charged particles as described by Frank et al. (2006) and for the DMA transfer function as described by Rose et al. (2008b). For the multiple charge correction we used the total aerosol particle number size distributions measured in parallel with the TDMPS. For several days TDMPS data were not available, and no charge correction was performed. Nevertheless, the CCN data from these days remained comparable with the others, because the effects of the charge correction were generally small (<5% change in activation diameters and other parameters used for further analysis).

The CCN efficiency spectra were also corrected for the differences in the counting efficiencies of the CCNC and the CPC. If the CCNC and CPC counting efficiencies were the same, a maximum activated fraction of $N_{CCN}/N_{CN} \approx 1$ would be expected for ammonium sulfate calibration aerosol particles at all supersaturation levels. As illustrated in Fig. 1, however, the measured maximum value of N_{CCN}/N_{CN} was close to one only for large particles. For smaller particles the measured maximum levels of N_{CCN}/N_{CN} decreased with decreasing particle size, which can be attributed to a decrease in the counting efficiency of the CCNC (most likely due to wall losses in the tubing inside the instrument). To correct for this bias, we have fitted an asymptotic function to the data points of the calibration efficiency spectra that reached at least 95% of their respective maximum values (red line in Fig. 1): $f_{corr} = x_1 - x_2 \cdot x_3^D$ with $x_1 = 1.00547$, $x_2 = 0.26208$, $x_3 = 0.98024$, $R^2 = 0.70881$. The inverse of this correction function was multiplied with all the atmospheric N_{CCN}/N_{CN} data points after the charge and transfer function corrections. In the following, for simplicity, the corrected CCN efficiency spectra are referred to as the "measured" CCN efficiency spectra.

The deviations of the highest N_{CCN}/N_{CN} measurement values from the counting efficiency correction function determined in the calibration experiments (f_{corr}, Fig. 1) indicate a relative uncertainty of ~5% for the CCN efficiencies determined for atmospheric aerosols (corrected CCN efficiency spectra). For the period after 20 July the relative

uncertainty increased to ∼10%, as indicated by a decrease in the observed maximum CCN efficiencies (offset in the CCNC flow rate).

2.2.4 Parameters derived from the CCN efficiency spectra

Basic spectral parameters

The measured CCN efficiency spectra were fitted with a cumulative Gaussian distribution function (CDF; Rose et al., 2008b):

$$f_{N_{CCN}/N_{CN}} = a \left(1 + \mathrm{erf} \left(\frac{D - D_a}{\sigma_a \sqrt{2}} \right) \right) \tag{1}$$

The following best-fit parameters were determined for each spectrum: the maximum activated fraction $MAF_f = 2a$, the midpoint activation diameter D_a, and the CDF standard deviation σ_a. The fit function was also used to calculate the 50% activation diameter D_{50} at which $N_{CCN}/N_{CN} = 0.5$. In addition to the 3-parameter CDF fits with varying a, D_a, and σ_a, we have also performed 2-parameter CDF fits which were forced to $MAF_f = 1$ by fixing the parameter a at 0.5 and varying only D_a and σ_a. For the midpoint activation diameters and CDF standard deviations obtained from these fits we use the symbols D_t and σ_t. In addition to the above CDF fit-based parameters, the CCN efficiency measured at the largest diameter of each spectrum (D_{max}) was also taken for further analysis and discussion: $MAF_m = N_{CCN}/N_{CN}$ at $D_{max} \approx 270$ nm.

Characteristic examples of atmospheric CCN efficiency spectra of atmospheric aerosols and the corresponding CDF fits and parameters are illustrated in Fig. 2. Figure 2a shows an "ideal" spectrum that is characteristic for internally mixed aerosols with homogeneous composition and hygroscopicity of the particles (similar to ammonium sulfate calibration aerosol). In this case, the observed CCN efficiencies reach up to one ($MAF_f \approx MAF_m \approx 1$), and the activation diameters and standard deviations derived from the 3-parameter and 2-parameter CDF fits are essentially the same ($D_a \approx D_{50} \approx D_t$; $\sigma_a \approx \sigma_t$).

At medium and high supersaturation (S=0.47–1.27%), most CCN efficiency spectra were qualitatively similar to the one in Fig. 2a. At low supersaturation (S=0.07–0.27%), however, most CCN efficiency spectra deviated from the "ideal" shape and looked like the exemplary spectrum displayed in Fig. 2b, which is characteristic for externally mixed aerosols.

In these cases, the highest observed CCN efficiencies remain well below one (MAF<1), which indicates an external mixture of CCN-active particles with CCN-inactive particles, whereby the difference in CCN activity is due to chemical composition and hygroscopicity (not particle size). Test experiments with different CCNC flow rates yielded the same result, indicating that the observed deviations of MAF from unity were not governed by potential kinetic limitations of water uptake in the CCNC.

For CCN efficiency spectra with MAF<1 the activation diameters and standard deviations derived from the 3-parameter and 2-parameter CDF fits are not the same: the 3-parameter fit results represent the average properties of the CCN active aerosol particle fraction, whereas the 2-parameter fit results approximate the overall properties of the external mixture of CCN-active and CCN-inactive particles.

The difference between unity and the maximum observed CCN efficiency ((1–MAF_m or 1–MAF_f, respectively) represents the fraction of externally mixed CCN-inactive particles at D_{max} or averaged over the diameter range of D_a to D_{max}, respectively. The CDF standard deviations are general indicators for the extent of external mixing and heterogeneity of particle composition in the investigated aerosol: σ_a characterizes the CCN-active particles in the size range around D_a, and σ_t characterizes the overall heterogeneity of CCN-active and -inactive particles in the size range around D_t. Under ideal conditions, the CDF standard deviations should be zero for an internally mixed, fully monodisperse aerosol with particles of homogeneous chemical composition. Even after correcting for the DMA transfer function, however, calibration aerosols composed of high-purity ammonium sulfate exhibit small non-zero σ_a values that correspond to ~3% of D_a and can be attributed to heterogeneities of the water vapor supersaturation profile in the CCNC or other non-idealities such as particle shape effects (Rose et

CCN in polluted air and biomass burning smoke

D. Rose et al.

Title Page

Abstract | Introduction

Conclusions | References

Tables | Figures

◄ | ►►

◄ | ►

Back | Close

Full Screen / Esc

Printer-friendly Version

Interactive Discussion

al., 2008b). Thus σ_a/D_a values close to ~3% indicate internally mixed CCN, whereas higher values indicate external mixtures of particles with different chemical composition and hygroscopicity, respectively.

Effective hygroscopicity parameters

As proposed by Petters and Kreidenweis (2007), an effective hygroscopicity parameter κ can be used to describe the influence of chemical composition on the CCN activity of aerosol particles, i.e. on their ability to absorb water vapor and act as CCN. Based on Köhler theory, κ relates the dry diameter of aerosol particles to the critical water vapor supersaturation, i.e. the minimum supersaturation required for cloud droplet formation. For a given supersaturation, κ allows calculating the critical dry particle diameter, i.e. the minimum diameter required for the particle to be CCN-active. According to measurements and thermodynamic models, κ is zero for insoluble materials like soot, ~0.1 for secondary organic aerosols, ~0.6 for ammonium sulfate and nitrate, and ~1 for sodium chloride and sea spray aerosols. The effective hygroscopicity of mixed aerosols can be approximated by a linear combination of the κ-values of the individual chemical components weighted by the volume or mass fractions. On average, continental and marine aerosols tend to cluster around $\kappa=0.3$ and $\kappa=0.7$, respectively (Andreae and Rosenfeld, 2008; Kreidenweis et al., 2008; Pöschl et al., 2008).

For all data pairs of supersaturation and activation diameter derived from the CCN efficiency spectra measured in this study, κ parameters were calculated from the following Köhler model equation (equivalent to Eq. 6 of Petters and Kreidenweis, 2007, and Eq. A30 of Rose et al., 2008b):

$$s = \frac{D_{\text{wet}}^3 - D^3}{D_{\text{wet}}^3 - D^3(1-\kappa)} \exp\left(\frac{4\,\sigma_{\text{sol}}\,M_w}{R\,T\,\rho_w\,D_{\text{wet}}}\right) \qquad (2)$$

κ was determined by inserting the observed activation diameter (D_a, D_{50} or D_t) for D and varying both κ and the droplet diameter D_{wet} until the saturation ratio s was at

CCN in polluted air and biomass burning smoke

D. Rose et al.

the same time equivalent to the prescribed supersaturation S and to the maximum of a Köhler model curve of CCN activation (numerical minimum search for $-s$ and for $|s-(1+S/100\%)|$ with Matlab "fminsearch" and start values of $\kappa=0.2$ and $D_{\text{wet}}=D$).

For the temperature we inserted $T=298.15\,\text{K}$, the droplet surface tension was approximated by that of water ($\sigma_{\text{sol}}=0.072\,\text{J}\,\text{m}^{-2}$), and the other parameters were set to $R=8.315\,\text{J}\,\text{K}^{-1}$ (gas constant), $\rho_w=997.1\,\text{kg}\,\text{m}^{-3}$ and $M_w=0.018015\,\text{kg}\,\text{mol}^{-1}$ (density and molar mass of water).

κ_a calculated from the data pairs of S and D_a characterizes the CCN-active particles in the size range around D_a. κ_t calculated from D_t characterizes the mixture of CCN-active and -inactive particles in the size range around D_t. κ_{50} calculated from D_{50} characterizes primarily the CCN-active particles in the size range around D_{50} but it is also influenced by the CCN-inactive fraction. It is less well-defined and meaningful than κ_a and κ_t, but it has been included for completeness and for comparison with other studies reporting only D_{50} as the CCN activation diameter (e.g. Kuwata et al., 2008).

CCN size distributions and number concentrations

CCN size distributions ($dN_{\text{CCN}}/d\log D$) were calculated by multiplying the CCN efficiency spectra (3-parameter CDF fits of $N_{\text{CCN}}/N_{\text{CN}}$) with the total aerosol particle (CN) number size distributions measured in parallel ($dN_{\text{CN}}/d\log D$). In these calculations, the fit parameter a was limited to a maximum value of 0.5 (MAF$_f$=1), because CCN concentrations exceeding CN concentrations are physically not realistic. Near the activation diameter, the size resolution of the CCN efficiency spectra was generally higher than that of the CN size distribution measurement data from the TDMPS ($d\log D=0.083$). Thus the CN size distributions were linearly interpolated on a grid with ten-fold smaller size steps.

Total CCN concentrations ($N_{\text{CCN,S}}$) were calculated by stepwise integration of the CCN size distributions with $d\log D=0.0083$ from 3 to 900 nm. Note that insufficient size-resolution near the activation diameter can lead to substantial deviations in the

CCN in polluted air and biomass burning smoke

D. Rose et al.

Full Screen / Esc

Printer-friendly Version

Interactive Discussion

calculation of total CCN number concentrations (up to ~10% at low S, up to ~5% at high S with $d\log D$=0.083 vs. $d\log D$=0.0083 in this study).

3 Results and discussion

3.1 CCN efficiency spectra and related parameters

During the 30 day campaign period of PRIDE-PRD2006, we measured ~2200 size-resolved CCN efficiency spectra (activation curves) for atmospheric aerosols at water vapor supersaturations in the range of 0.07% to 1.27%. Exemplary spectra are shown in Fig. 2, and the derivation and interpretation of characteristic parameters is explained in Sect. 2.2.4.

3.1.1 Campaign averages

Figure 3 shows campaign averages of the atmospheric CCN efficiency spectra at the six investigated supersaturation levels. The average parameters derived from the CCN efficiency spectra are summarized in Table 2, and their statistical distributions are illustrated in the online supplementary material: http://www.atmos-chem-phys-discuss. net/8/17343/2008/acpd-8-17343-2008-supplement.pdf (Figs. S1–S6).

As expected, the midpoint activation diameters D_a increased with S and were larger than the critical dry diameters for CCN activation of pure ammonium sulfate particles at the same supersaturation levels. At medium and high supersaturation (S=0.47–1.27%), the CCN efficiency spectra generally reached up to one (MAF$_f$≈1) and the relative standard deviations of the 3-parameter CDF fits were small (σ_a/D_a≈10%), which implies that nearly all aerosol particles larger than the midpoint activation diameter (D>D_a) were CCN-active. At low supersaturation (S=0.07–0.27%), however, the maximum activated fractions remained on average well below one, which indicates a substantial proportion (1–MAF$_f$) of externally mixed CCN-inactive particles with much

lower hygroscopicity. At S=0.07%, the average MAF$_f$ was only ~0.75 with minimum values as low as ~0.4, i.e. even at diameters as large as ~250 nm an average of ~25% and up to ~60% of the aerosol particles were not CCN-active. To our knowledge such high proportions of externally mixed CCN-inactive particles have not been observed before in atmospheric aerosols.

Sensitivity tests with the κ-Köhler model described in Sect. 2.2.4 (Petters and Kreidenweis, 2007) indicate that particles as large as ~250 nm must have an effective hygroscopicity parameter κ<0.1 to be not activated at S=0.07%. On the other hand, $S \approx 0.7$% would be required to activate 300 nm particles that are wettable but completely insoluble and non-hygroscopic (κ=0). Most likely the CCN-inactive particles were freshly emitted (non-aged/non-coated) soot particles with $\kappa \approx 0.01$, which will be detailed and discussed further in a follow-up study based on Volatility Tandem DMA (VTDMA) and chemical composition data (Rose et al., 2008a). Other recent studies from PRIDE-PRD2006 (Garland et al., 2008b) and from a similar field campaign in the vicinity of Beijing (Cheng et al., 2008; Garland et al., 2008a; Wehner et al., 2008; Wiedensohler et al., 2008) also indicate strong regional pollution with large proportions and external mixtures of soot particles in the atmospheric aerosol near Chinese mega-cities and city-clusters.

Figure 4a gives an overview of the maximum activated fractions (MAF$_f$) and normalized standard deviations (σ_a/D_a) of the 3-parameter CDF fits as well as the normalized standard deviations of the 2-parameter CDF fits (σ_t/D_t) to the measured CCN efficiency spectra. The average parameter values are plotted against the corresponding average midpoint activation diameters (D_a, D_t) that have been observed at the six prescribed levels of water vapor supersaturation (S=0.07–1.27%).

As detailed in Sect. 2.2.4, σ_a/D_a characterizes the heterogeneity of CCN-active particles in the size range around D_a, whereas σ_t/D_t characterizes the overall heterogeneity of aerosol particles in the size range around D_t.

For small particles in the nucleation or Aitken size range (~30–70 nm), the heterogeneity parameters σ_a/D_a and σ_t/D_t were nearly identical and close to ~10%. This is

clearly higher than the ~3% observed for aerosols of homogeneous chemical composition (e.g. pure ammonium sulfate), indicating that the particles in this size range were not fully internally mixed with respect to their solute content. For larger particles in the accumulation size range (~70–200 nm), σ_a/D_a remained at ~10% whereas σ_t/D_t in-
5 creased strongly up to ~25% at ~200 nm. This confirms that the CCN-active particles in the accumulation size range had fairly homogeneous properties but were externally mixed with CCN-inactive particles.

Figure 4b gives an overview of the effective hygroscopicity parameters (κ_a, κ_t) that have been derived from the midpoint activation diameters (D_a, D_t) of the 3-parameter
10 and 2-parameter CDF fits, respectively. As detailed in Sect. 2.2.4, κ_a calculated from S and D_a characterizes the average hygroscopicity of CCN-active particles in the size range around D_a, whereas κ_t calculated from S and D_t characterizes the average hygroscopicity of the total ensemble of aerosol particles in the size range around D_t.

For small particles in the nucleation or Aitken size range (~30–70 nm), κ_a and κ_t
15 were nearly identical and close to ~0.3. For larger particles in the accumulation size range (~70–200 nm), however, κ_a increased substantially to ~0.4–0.5, whereas κ_t increased only slightly to ~0.35.

Overall, larger particles were on average more hygroscopic but also more heterogeneous than smaller particles. The observed values of κ_a, κ_t, σ_a/D_a, σ_t/D_t, and MAF$_f$
20 suggest that the particles in the nucleation or Aitken size range were mostly composed of organics and sulfate and largely but not fully internally mixed, whereas the particles in the accumulation size range consisted mostly of an external mixture of soot particles ($\kappa < 0.1$; ~25% at ~200 nm) and sulfate-rich particles ($\kappa \approx 0.4$–0.5; ~75% at ~200 nm). Note that the properties of large accumulation mode particles are not only
25 important for cloud formation at low and medium supersaturation (low and moderate updraft velocities; Segal and Khain, 2006; Reutter et al., 2008) but also for aerosol optical properties and direct radiative effects on climate (Garland et al., 2008b). These and other aspects of aerosol chemical composition and mixing state will be further explored and discussed in more detail in a follow up study (Rose et al., 2008a). Averaged

CCN in polluted air and biomass burning smoke

D. Rose et al.

over all diameters, the mean hygroscopicity parameter values for the entire campaign were κ_a=0.34 and κ_t=0.30 (Table 2).

3.1.2 Time series and biomass burning event

Figure 5 shows time series of characteristic parameters (D_a, D_t, MAF$_f$, MAF$_m$, σ_a, σ_t, σ_a/D_a, σ_t/D_t, κ_a, κ_t) derived from the atmospheric CCN efficiency spectra measured throughout the campaign. For clarity, the parameters in Fig. 5c–j are shown only for the smallest and largest supersaturations that were measured during the entire campaign (S=0.07%, S=0.87%). The temporal evolution of most parameters at S=0.07% was qualitatively similar to S=0.27%, and that at S=0.87% was representative for S=0.47– 1.27%.

Most parameters exhibited pronounced diurnal cycles which are consistent with the results of other recent studies from PRIDE-PRD2006 (Garland et al., 2008b; Hua et al., 2008b). The diurnal cycles in CCN properties will be described and discussed together with the variability of other aerosol properties including chemical composition, volatility, and optical parameters in a follow up study (Rose et al., 2008a). As illustrated in Fig. 5i and j, both the fitted and the measured maximum activated fractions (MAF$_f$, MAF$_m$) dropped by ~10% after 20 July, which is most likely due to a measurement artifact (offset in the flow rate of the CCNC).

In addition to the diurnal variability, several CCN parameters exhibited pronounced changes during high pollution events. Especially on 23–26 July, the midpoint activation diameters and standard deviations of the CDF fits increased and the hygroscopicity parameters decreased relative to the campaign average (Fig. 5, panels a–h). The changes indicate an increase in the proportion of particulate matter with low hygroscopicity (organic substances) and in the heterogeneity of particles (external mixing), and they were most pronounced for small particles (~30–80 nm; $S \geq$ 0.27%).

The highly polluted period of 23–26 July 2006 was characterized by intense local biomass burning and very high aerosol mass concentrations (Garland et al., 2008b). During this period, the source of the pollution was evident and unique: the burning of

CCN in polluted air and biomass burning smoke

D. Rose et al.

Title Page

Abstract | Introduction

Conclusions | References

Tables | Figures

◄ | ►

◄ | ►

Back | Close

Full Screen / Esc

Printer-friendly Version

Interactive Discussion

plant waste by local farmers was visible in the vicinity surrounding the measurement site, and it was the only time that such intense local biomass burning and pollution occurred during the campaign. The observation of heavy biomass burning event started after a power outage in the evening of 22 July and ended by heavy rainfalls beginning at ~13:00 on 26 July. Thus the period of 23 July 00:00–26 July 12:59 will be referred to as the "biomass burning event (BBE)". The average CCN parameters for this period are summarized in Table 2.

Figure 6 shows the CCN efficiency spectra averaged over the biomass burning event (red), over the entire campaign (black) and over the entire campaign excluding the biomass burning event (green). During the BBE, the CCN efficiency spectra were shifted towards larger particle sizes for all supersaturations, reflecting lower CCN activity than during the rest of the campaign. The increase of D_a was most pronounced for S=0.67% (+25% during the BBE) and least different for S=0.07% and S=1.27% (+10% during the BBE). Moreover, for all supersaturations except 0.07%, the standard deviations of the CDF fits and heterogeneity parameters (σ/D), respectively, increased by factors up to ~2, indicating a strong increase in heterogeneity of small particles (30–100 nm, Table 2). Only the maximum activated fractions did not change significantly during the biomass burning event, i.e. the externally mixed fraction of particles that could not be activated at low S remained the same. The average spectra for the entire campaign and for the campaign excluding the biomass burning did hardly differ from each other.

Figure 7 gives an overview of the effective hygroscopicity parameters (κ_a, κ_t) that have been derived from the midpoint activation diameters (D_a, D_t) averaged over the entire campaign and over the biomass burning event. Figure 7a shows that during the BBE the average hygroscopicity of CCN-active particles was substantially reduced at all sizes. Averaged over all diameters, the mean value of κ_a during the BBE was ~30% lower than during the rest of the campaign: 0.24 vs. 0.34 (Table 2).

As illustrated in Fig. 7b, the average hygroscopicity of the total aerosol, including CCN-active and -inactive particles, was also strongly reduced for small particles

Printer-friendly Version

Interactive Discussion

(<100 nm) but not so much for large particles (~200 nm). Averaged over all diameters, however, the mean value of κ_t during the BBE was also ~30% lower than during the rest of the campaign: 0.21 vs. 0.30 (Table 2).

To our knowledge, these are the first size-resolved CCN field measurement data and hygroscopicity parameters reported for freshly emitted biomass burning smoke in the atmosphere. They are consistent with earlier lab studies reporting low hygroscopicity of freshly emitted biomass burning particles (Rissler et al., 2006; Andreae and Rosenfeld, 2008).

3.2 CCN size distributions and number concentrations

Figure 8 shows total aerosol particle (CN) and CCN number size distributions averaged over the entire campaign and over the biomass burning event, respectively. The corresponding averages of the total CCN number concentrations ($N_{CCN,S}$) and of the total CCN efficiencies ($N_{CCN,S}/N_{CN,tot}$) are summarized in Table 2.

As illustrated in Fig. 8a, the average CN size distribution for the entire campaign was monomodal with a maximum at ~75 nm, and the corresponding total particle number concentration was $N_{CN,tot}=1.8\times10^4$ cm^{-3} (Table 2). At S=0.07% the CCN size distribution accounted only for ~5% of $N_{CN,tot}$, because only a minor fraction of the CN were larger than the activation diameter (~200 nm). At S=0.27–0.87% the CCN activation diameters were close to the maximum of the CN number mode and the integral CCN efficiencies were substantially higher ($N_{CCN,S}/N_{CN,tot}$=35–74%; Table 2). During the biomass burning event (Fig. 8b), the CN size distribution was broader and the maximum was shifted to larger sizes (~120 nm, a value typical of biomass smoke; Reid et al., 2005). The average number concentration of CN was slightly smaller (~1.5×10^4 cm^{-3}), but due to the larger average particle sizes the CCN number concentrations at S=0.07% and 0.27% were much higher (+70% and +15%, respectively). For S≥0.47%, however, $N_{CCN,S}$ decreased compared to the rest of the campaign (Table 2).

Figure 9 shows time series of $N_{CN,tot}$, $N_{CCN,S}$ and $N_{CCN,S}/N_{CN,tot}$ throughout the cam-

paign. The values of $N_{CN,tot}$ as well as of $N_{CCN,S}$ exhibited high temporal variability over the ranges of $\sim 10^3$–4×10^4 cm^{-3} for $N_{CN,tot}$ and $\sim 10^2$–3×10^3 cm^{-3}, $\sim 10^3$–2×10^4 cm^{-3}, and $\sim 3 \times 10^3$–3×10^4 cm^{-3} for $N_{CCN,S}$ at S=0.07%, 0.27%, and 0.87%, respectively. Box plots illustrating the statistical distribution are given in the online supplement (Fig. S6), and the corresponding mean values and standard deviations are listed in Table 2. To our knowledge, these are the highest CCN number concentrations that have been measured and reported so far (Andreae, 2008; Andreae and Rosenfeld, 2008; Wieden-sohler et al., 2008).

The trend of $N_{CN,tot}$ was generally followed by $N_{CCN,S}$ at $S \geq 0.47$%, but not at S=0.07–0.27%. During the biomass burning event, for instance, $N_{CCN,S}$ at S=0.07% reached its highest level, whereas $N_{CN,tot}$ exhibited medium to low values (Fig. 9a), resulting in a pronounced maximum of the integral CCN efficiency $N_{CCN,S}/N_{CN,tot}$ (Fig. 9b).

3.3 Prediction of CCN number concentration

In this section we compare different model approaches for the approximation/prediction of CCN concentration as a function of water vapor supersaturation, aerosol particle number concentration, size distribution and hygroscopicity: 1) the classical power law approach relating $N_{CCN,S}$ to $N_{CCN,1}$, i.e. to the CCN concentration at S=1%; 2) a modified power law approach relating $N_{CCN,S}$ to the concentration of aerosol particles with D>30 nm ($N_{CN,30}$); and 3) the κ-Köhler model approach relating $N_{CCN,S}$ to the aerosol particle size distribution ($dN_{CN}/d\log D$) and hygroscopicity. For all data points obtained during the campaign, the model results were compared with the measurement results, and the mean values of the relative deviations are summarized in Table 3.

3.3.1 Classical power law

Figure 10 shows the average values of $N_{CCN,S}$ plotted against S and a power law fit of the form $N_{CCN,S}=N_{CCN,1}\cdot(S/(1\%))^k$ (Pruppacher and Klett, 1997). The obtained fit

parameter $N_{CCN,1} \approx 1.4 \times 10^4$ cm^{-3} is substantially higher than any previously reported value, and $k \approx 0.65$ is within the range of values reported for other continental locations (0.4–0.9; Pruppacher and Klett, 1997; Andreae, 2008). The relative deviations of the measured data points from the power law were on average in the range of 40–80% for $S=0.27–1.27\%$ but as high as 270% for $S=0.07\%$ (Table 3).

3.3.2 Modified power law

Figure 11 shows all measured values of $N_{CCN,S}$ plotted against $N_{CN,30}$ and power law fits of the form $N_{CCN,S}=N_{CN,30} \cdot s^{-q}$ with $s=1+S/(100\%)$. An overview of the q values and correlation coefficients is given in Table 4. In this approach, CN with $D<30$ nm were excluded, because they are generally not CCN-active and highly variable due to new particle formation (nucleation events). Moreover, the water vapor saturation ratio s was used instead of the supersaturation S, because the exponent varies more regularly with s than with S (Table 4: monotonous dependence of q on s vs. non-monotonous dependence of Q on S). At high supersaturations ($S \geq 0.47\%$), $N_{CCN,S}$ was closely correlated to $N_{CN,30}$ ($R^2=0.80–0.98$), and the mean relative deviations between the power law fit and the measured values of $N_{CCN,S}$ were only 4–27% (Table 3). At $S=0.27\%$ the correlation was much worse ($R^2=0.61$, mean deviation 40%), and at $S=0.07\%$ there was practically no correlation and the individual $N_{CCN,S}$ data points deviated by up to one order of magnitude from the power law fit ($R^2=0.09$, mean deviation 59%).

3.3.3 κ-Köhler model

In Fig. 12, predicted CCN number concentrations ($N_{CCN,S,p}$) that were obtained with the κ-Köhler model and different hygroscopicity parameters are plotted against measured values of $N_{CCN,S}$. $N_{CCN,S,p}$ was calculated by integrating the measured CN size distribution above the critical dry particle diameter for CCN activation that corresponds to the given values of κ and S (Sects. 2.2.4 and 3.2).

As illustrated in Fig. 12a, the predicted and measured values of $N_{\mathrm{CCN,S}}$ are in very good agreement, when for each data point κ_t was taken from the CCN efficiency spectrum measured in parallel to the CN size distribution. With this approach, the mean relative deviation averaged over all supersaturations was only 7%, and the overall mean bias of the model values was +5% (Table 3; largest deviations and bias at low S). The agreement demonstrates that κ_t indeed reflects the average hygroscopicity of the investigated atmospheric aerosol particles. The time series in Fig. 13a shows that the relative deviations between predicted and measured $N_{\mathrm{CCN,S}}$ were generally positive and less than 20%.

Fair agreement was also achieved when the campaign average value of $\kappa_t=0.30$ and the corresponding constant activation diameters for the prescribed supersaturation levels (210, 86, 59, 47, 39, and 30 nm; $S=0.07$–1.27%) were used for the calculation of $N_{\mathrm{CCN,S}}$ from the individual measured CN size distributions. With this approach, the overall mean relative deviation was twice as high but the bias was hardly higher than when using individual κ_t values (13% and +6%, respectively; Table 3; Fig. 12b). Note that the campaign average value of κ_t equals the average value of hygroscopicity parameters observed or inferred for other continental locations (Andreae and Rosenfeld, 2008; Pöschl et al., 2008).

As illustrated by the time series in Fig. 13b, the approach using a constant average value of $\kappa=0.3$ cannot fully account for the observed temporal variations in aerosol composition and CCN properties. It yields relative deviations in the range of −40% to +80% of $N_{\mathrm{CCN,S}}$. Under most circumstances, however, i.e. for 77% of all data points, the deviations were still less than ±20%, which appears quite reasonable for data that span more than two orders of magnitude. Even during the BBE, which was characterized by ∼30% lower hygroscopicity parameters ($\kappa_t\approx0.2$; Sect. 3.1.2), the average deviation between predicted and measured $N_{\mathrm{CCN,S}}$ was only 20%. The regular pattern of positive and negative deviations observed during the rest of the campaign can be attributed to pronounced diurnal cycles of aerosol composition and CCN properties (Rose et al., 2008a).

CCN in polluted air and biomass burning smoke

D. Rose et al.

With all other types of hygroscopicity parameters (average or individual values of κ_a and κ_{50}), the positive bias was higher than with κ_t (9–14%, Table 3), and the relative deviations were of similar magnitude as with constant κ_t=0.3 (10–16%, Table 3).

4 Summary and conclusions

5 The dry CCN activation diameters measured during PRIDE-PRD2006 at S=0.07–1.27% were in the range of 30–200 nm, corresponding to effective hygroscopicity parameters κ in the range of 0.1–0.5. The mean value of κ characterizing the hygroscopicity of all aerosol particles averaged over the whole campaign and investigated size range was 0.3, which equals the average value of κ observed or inferred for other
10 continental locations (Andreae and Rosenfeld, 2008; Pöschl et al., 2008). Particles in the nucleation or Aitken size range ($D\approx$30–70 nm, $\kappa\approx$0.25) were on average less hygroscopic than particles in the accumulation size range ($D\approx$70–200 nm, $\kappa\approx$0.35).

During a strong local biomass burning event (BBE) the aerosol particles were generally less CCN active (∼10% larger activation diameters, mean $\kappa\approx$0.2), and in partic-
15 ular the hygroscopicity of small particles decreased more than that of large particles ($\kappa\approx$0.15 for $D\approx$30–100 nm; $\kappa\approx$0.3 for $D\approx$200 nm). The small particles were also more heterogeneously mixed as indicated by an increase in the width of the CCN efficiency spectra (up to twofold increase of heterogeneity parameter σ/D). Due to the very intense local sources and high level of pollution, the κ values observed during the BBE
20 can be regarded as characteristic for freshly emitted smoke from the open burning of agricultural waste.

At low S (≤0.27%), the maximum activated fraction remained generally well below one, which indicates substantial proportions of externally mixed CCN-inactive particles with much lower hygroscopicity ($\kappa\approx$0.01) – most likely soot particles.
25 At S=0.07%, the average MAF$_f$ was only ∼0.75 with minimum values as low as ∼0.4, i.e. even at diameters as large as ∼250 nm an average of ∼25% and up to ∼60% of the aerosol particles were not CCN-active. To our knowledge such high proportions of

CCN in polluted air and biomass burning smoke

D. Rose et al.

externally mixed CCN-inactive particles have not been observed before in atmospheric aerosols. Note, however, that these CCN-inactive particles contributed only around ~3% to the total aerosol particle number concentration. The integral CCN efficiencies at moderate supersaturations ($N_{CCN,S}/N_{CN,tot} \approx 0.36$–$0.53$ at $S = 0.27\%$–0.47%, Table 2) were even slightly higher than the global average value reported by Andreae (2008) ($N_{CCN,S}/N_{CN,tot} \approx 0.36$ at $S = 0.4\%$).

From the measured CCN efficiency spectra and total aerosol particle (CN) size distributions, we derived CCN size distributions and total CCN number concentrations ($N_{CCN,S}$). On average, $N_{CCN,S}$ ranged from $1100\,\text{cm}^{-3}$ at $S = 0.07\%$ to $16\,000\,\text{cm}^{-3}$ at $S = 1.27\%$, representing ~7% to ~85% of the total aerosol particle number concentration ($N_{CN,tot}$). During the biomass burning event, the CN size distribution was broader and the maximum was shifted to larger sizes (from ~75 nm to ~120 nm). The average number concentration of CN was slightly smaller (~$1.5 \times 10^4\,\text{cm}^{-3}$ vs. ~$1.8 \times 10^4\,\text{cm}^{-3}$), but due to the larger average particle sizes the CCN concentrations at low supersaturation were substantially higher (+100% at $S = 0.07\%$, +10% at $S = 0.27\%$). For high supersaturations ($S \geq 0.47\%$), however, $N_{CCN,S}$ decreased by up to ~30% compared to the rest of the campaign.

Based on the measurement data, we have tested different model approaches (power laws and κ-Köhler models) for the approximation/prediction of $N_{CCN,S}$ as a function of water vapor supersaturation, aerosol particle number concentration, size distribution and hygroscopicity. Depending on S and on the applied type of power law or hygroscopicity parameter, the relative deviations between measured and predicted $N_{CCN,S}$ can range from a few percent to several hundred percent. The largest deviations occurred at low S and with power laws based on particle number concentration without size information. Much better predictions could be made when using measured aerosol size distributions in combination with κ-Köhler models.

With variable κ values obtained from individual CCN efficiency spectra, the relative deviations between measured and predicted $N_{CCN,S}$ were on average less than ~10% and did hardly exceed 20%. These results confirm the applicability of the κ-

Köhler model approach for efficient description of the CCN properties of atmospheric aerosols. Note, however, that in case of externally mixed CCN-active and -inactive aerosol particles, the use of κ parameters derived from different types of fits to the measured CCN efficiency spectra (2- or 3-parameter CDF) can lead to substantially different results – especially at low S (increase of deviations by up to a factor of $\sim$4).

Assuming a constant average value of $\kappa=0.3$, the deviations were on average still less than $\sim$20%, which confirms earlier studies indicating that "size matters more than chemistry" for the CCN activity of aerosol particles (Dusek et al., 2006) and that $\kappa=0.3$ may be suitable for approximating the hygroscopicity and CCN activity of continental aerosols in large scale models of the atmosphere and climate. On the other hand, temporal variations such as the observed biomass burning event and diurnal cycles led to relative deviations of up to 80%, which cannot be captured with a constant hygroscopicity parameter.

The publication of this article is financed by the Max Planck Society.

MAX-PLANCK-GESELLSCHAFT

References

Andreae, M. O.: Correlation between cloud condensation nuclei concentration and aerosol optical thickness in remote and polluted regions, Atmos. Chem. Phys. Discuss., 8, 11 293–

Title Page

Abstract | Introduction

Conclusions | References

Tables | Figures

◀ | ▶

◀ | ▶

Back | Close

Full Screen / Esc

Printer-friendly Version

Interactive Discussion

11 320, 2008,
http://www.atmos-chem-phys-discuss.net/8/11293/2008/.

Andreae, M. O. and Rosenfeld, D.: Aerosol-cloud-precipitation interactions. Part 1. The nature and sources of cloud-active aerosols, Earth Sci. Rev., 89, 13–41, 2008.

Andreae, M. O., Schmid, O., Yang, H., Yu, J., Zeng, L., and Zhang, Y.: Optical properties and chemical composition of the atmospheric aerosol in urban Guangzhou, China, Atmos. Environ., 42, 6335–6350, doi:10.1016/j.atmosenv.2008.01.030, 2008.

Cheng, Y. F., Berghof, M., Garland, R. M., Wiedensohler, A., Wehner, B., Su, H., Achtert, P., Nowak, A., Pöschl, U., Zhang, Y. H., Zhu, T., and Zeng, L. M.: Influence of soot mixing state on aerosol light absorption at a polluted regional site in North-Eastern China, J. Geophys. Res.-Atmos., submitted, 2008.

Deng, X., Tie, X., Wu, D., Zhou, X., Bi, X., Tan, H., Li, F., and Jiang, C.: Long-term trend of visibility and its characterizations in the Pearl River Delta (PRD) region, China, Atmos. Environ., 42, 1424–1435, 2008.

Dusek, U., Frank, G. P., Hildebrandt, L., Curtius, J., Schneider, J., Walter, S., Chand, D., Drewnick, F., Hings, S., Jung, D., Borrmann, S., and Andreae, M. O.: Size matters more than chemistry for cloud nucleating ability of aerosol particles, Science, 312, 1375–1378, 2006.

Fan, S., Wang, B., Tesche, M., Engelmann, R., Althausen, A., Liu, J., Zhu, W., Fan, Q., Li, M.-H., Ta, N., Song, L., and Leong, K.: Meteorological conditions and structures of atmospheric boundary layer in October 2004 over Pearl River Delta area, Atmos. Environ., 42, 6174–6186, 2008.

Frank, G. P., Dusek, U., and Andreae, M. O.: Technical note: A method for measuring size-resolved CCN in the atmosphere, Atmos. Chem. Phys. Discuss., 6, 4879–4895, 2006,
http://www.atmos-chem-phys-discuss.net/6/4879/2006/.

Garland, R. M., Schmid, O., Nowak, A., Achtert, P., Wiedensohler, A., Gunthe, S. S., Takegawa, N., Kita, K., Kondo, Y., Hu, M., Shao, M., Zeng, L. M., Zhu, T., Andreae, M. O., and Pöschl, U.: Aerosol optical properties observed during CAREBeijing-2006: Characteristic differences between the inflow and outflow of Beijing city air, J. Geophys. Res.-Atmos., submitted, 2008a.

Garland, R. M., Yang, H., Schmid, O., Rose, D., Nowak, A., Achtert, P., Wiedensohler, A., Takegawa, N., Kita, K., Miyazaki, Y., Kondo, Y., Hu, M., Shao, M., Zeng, L. M., Zhang, Y. H., Andreae, M. O., and Pöschl, U.: Aerosol optical properties in a rural environment near

CCN in polluted air and biomass burning smoke

D. Rose et al.

Title Page

Abstract | Introduction

Conclusions | References

Tables | Figures

|◄ | ►|

◄ | ►

Back | Close

Full Screen / Esc

Printer-friendly Version

Interactive Discussion

the mega-city Guangzhou, China: implications for regional air pollution, radiative forcing and remote sensing, Atmos. Chem. Phys., 8, 5161–5186, 2008b, http://www.atmos-chem-phys.net/8/5161/2008/.

Hagler, G. S., Bergin, M. H., Salmon, L. G., Yu, J. Z., Wan, E. C. H., Zheng, M., Zeng, L. M., Kiang, C. S., Zhang, Y. H., Lau, A. K. H., and Schauer, J. J.: Source areas and chemical composition of fine particulate matter in the Pearl River Delta region of China, Atmos. Environ., 40, 3802–3815, 2006.

Hua, W., Chen, Z. M., Jie, C. Y., Kondo, Y., Hofzumahaus, A., Takegawa, N., Lu, K. D., Miyazaki, Y., Kita, K., Wang, H. L., Zhang, Y. H., and Hu, M.: Atmospheric hydrogen peroxide and organic hydroperoxides during PRIDE-PRD'06, China: their concentration, formation mechanism and contribution to secondary aerosols, Atmos. Chem. Phys. Discuss., 8, 10 481–10 530, 2008, http://www.atmos-chem-phys-discuss.net/8/10481/2008/.

Huang, Y., Chameides, W. L., and Dickinson, R. E.: Direct and indirect effects of anthropogenic aerosols on regional precipitation over east Asia, J. Geophys. Res., 112, D03212, doi:10.1029/2006JD007114, 2007.

IAPSAG: WMO/IUGG International Aerosol Precipitation Science Assessment Group (IAPSAG) Report: Aerosol Pollution Impact on Precipitation: A Scientific Review, World Meteorological Organization, Geneva, 482, 2007.

IPCC: Climate Change 2007: The Physical Science Basis, Contribution of Working Group I to the Fourth Assessment Report of the Intergovernmental Panel on Climate Change, edited by: Solomon, S., Qin, D., Manning, M., Chen, Z., Marquis, M., Averyt, K., Tignor, M., and Miller, H. L., Cambridge University Press, Cambridge and New York, 996, 2007.

Kreidenweis, S. M., Petters, M. D., and Chuang, P. Y.: Cloud particle precursors, Clouds in the Perturbed Climate System: Their Relationship to Energy Balance, Atmospheric Dynamics, and Precipitation. Strüngmann Forum Report, vol. 2, edited by: Heintzenberg, J. and Charlson, R. J., The MIT Press, Cambridge, MA, 2008.

Kuwata, M., Kondo, Y., Mochida, M., Takegawa, N., and Kawamura, K.: Dependence of CCN activity of less volatile particles on the amount of coating observed in Tokyo, J. Geophys. Res.-Atmos., 112, D11207, doi:10.1029/2006JD007758, 2007.

Kuwata, M., Kondo, Y., Miyazaki, Y., Komazaki, Y., Kim, J. H., Yum, S. S., Tanimoto, H., and Matsueda, H.: Cloud condensation nuclei activity at Jeju Island, Korea in spring 2005, Atmos. Chem. Phys., 8, 2933–2948, 2008,

CCN in polluted air and biomass burning smoke

D. Rose et al.

http://www.atmos-chem-phys.net/8/2933/2008/.

Lance, S., Medina, J., Smith, J. N., and Nenes, A.: Mapping the Operation of the DMT Continuous Flow CCN Counter, Aerosol Sci. Technol., 40, 242–254, 2006.

Li, Z. Q., Xia, X., Cribb, M., Mi, W., Holben, B., Wang, P., Chen, H., Tsay, S. C., Eck, T. F., Zhao, F., Dutton, E. G., and Dickerson, R. E.: Aerosol optical properties and their radiative effects in northern China, J. Geophys. Res., 112, D22S01, doi:10.1029/2006JD007382, 2007.

Liu, B. H., Xu, M., Henderson, M., Qi, Y., and Li, Y. Q.: Taking China's temperature: Daily range, warming trends, and regional variations, 1955–2000, J. Climate, 17, 4453–4462, 2004.

Liu, X. G., Cheng, Y. F., Zhang, Y. H., Jung, J. S., Sugimoto, N., Chang, S. Y., Kim, Y. J., Fan, S. J., and Zeng, L. M.: Influences of relative humidity and particle chemical composition on aerosol scattering properties during the 2006 PRD campaign, Atmos. Environ., 42, 1525–1536, 2008.

Massie, S. T., Torres, O., and Smith, S. J.: Total Ozone Mapping Spectrometer (TOMS) observations of increases in Asian aerosol in winter from 1979 to 2000, J. Geophys. Res.-Atmos., 109, D18211, doi:10.1029/2004JD004620, 2004.

Matsumoto, K., Tanaka, H., Nagao, I., and Ishizaka, Y.: Contribution of particulate sulfate and organic carbon to cloud condensation nuclei in the marine atmosphere, Geophys. Res. Lett., 24, 655–658, 1997.

McFiggans, G., Artaxo, P., Baltensperger, U., Coe, H., Facchini, M. C., Feingold, G., Fuzzi, S., Gysel, M., Laaksonen, A., Lohmann, U., Mentel, T. F., Murphy, D. M., O'Dowd, C. D., Snider, J. R., and Weingartner, E.: The effect of physical and chemical aerosol properties on warm cloud droplet activation, Atmos. Chem. Phys., 6, 2593–2649, 2006, http://www.atmos-chem-phys.net/6/2593/2006/.

Petters, M. D. and Kreidenweis, S. M.: A single parameter representation of hygroscopic growth and cloud condensation nucleus activity, Atmos. Chem. Phys., 7, 1961–1971, 2007, http://www.atmos-chem-phys.net/7/1961/2007/.

Pöschl, U., Rose, D., and Andreae, M. O.: Climatologies of Cloud-related Aerosols: Part 2: Particle Hygroscopicity and Cloud Condensation Nuclei Activity, Clouds in the Perturbed Climate System: Their Relationship to Energy Balance, Atmospheric Dynamics, and Precipitation. Strüngmann Forum Report, vol. 2, edited by: Heintzenberg, J. and Charlson, R. J., The MIT Press, Cambridge, MA, 2008.

Pruppacher, H. R. and Klett, J. D.: Microphysics of clouds and precipitation, Kluwer Academic Publishers, Dordrecht, 288–289, 1997.

CCN in polluted air and biomass burning smoke

D. Rose et al.

Title Page

Abstract	Introduction
Conclusions	References
Tables	Figures

◄ | ►

◄ | ►

Back | Close

Full Screen / Esc

Printer-friendly Version

Interactive Discussion

Qian, Y., Kaiser, D. P., Leung, L. R., and Xu, M.: More frequent cloud-free sky and less surface solar radiation in China from 1955 to 2000, Geophys. Res. Lett., 33, L01812, doi:10.1029/2005GL024586, 2006.

Reid, J. S., Koppmann, R., Eck, T. F., and Eleuterio, D. P.: A review of biomass burning emissions part II: intensive physical properties of biomass burning particles, Atmos. Chem. Phys., 5, 799–825, 2005,
http://www.atmos-chem-phys.net/5/799/2005/.

Reutter, P., Trentmann, J., Simmel, M., Wernli, H., Andreae, M. O., and Pöschl, U.: Aerosol activation in pyro-clouds and smoky conditions, Atmos. Chem. Phys. Discuss., in preparation, 2008.

Richter, A., Burrows, J. P., Nuss, H., Granier, C., and Niemeier, U.: Increase in tropospheric nitrogen dioxide over China observed from space, Nature, 437, 129–132, 2005.

Rissler, J., Vestin, A., Swietlicki, E., Fisch, G., Zhou, J., Artaxo, P., and Andreae, M. O.: Size distribution and hygroscopic properties of aerosol particles from dry-season biomass burning in Amazonia, Atmos. Chem. Phys., 6, 471–491, 2006,
http://www.atmos-chem-phys.net/6/471/2006/.

Roberts, G. C. and Nenes, A.: A Continuous-Flow Streamwise Thermal-Gradient CCN Chamber for Atmospheric Measurements, Aerosol Sci. Technol., 39, 206–221, 2005.

Rose, D., Garland, R. M., Yang, H., Berghof, M., Wehner, B., Wiedensohler, A., Takegawa, N., Kondo, Y., Andreae, M. O., and Pöschl, U.: Cloud condensation nuclei in polluted air and biomass burning smoke near the mega-city Guangzhou, China – Part 2: CCN composition and diurnal cycles, Atmos. Chem. Phys. Discuss., in preparation, 2008a.

Rose, D., Gunthe, S. S., Mikhailov, E., Frank, G. P., Dusek, U., Andreae, M. O., and Pöschl, U.: Calibration and measurement uncertainties of a continuous-flow cloud condensation nuclei counter (DMT-CCNC): CCN activation of ammonium sulfate and sodium chloride aerosol particles in theory and experiment, Atmos. Chem. Phys., 8, 1153–1179, 2008b,
http://www.atmos-chem-phys.net/8/1153/2008/.

Rosenfeld, D., Dai, J., Yu, X., Yao, Z., Xu, X., Yang, X., and Du, C.: Inverse relations between amounts of air pollution and orographic precipitation, Science, 315, 1396–1398, 2007.

Rosenfeld, D., Lohmann, U., Raga, G. B., O'Dowd, C. D., Kulmala, M., Fuzzi, S., Reissell, A., and Andreae, M. O.: Flood or Drought: How Do Aerosols Affect Precipitation?, Science, 321, 1309–1313, 2008.

Segal, Y. and Khain, A.: Dependence of droplet concentration on aerosol conditions in different

CCN in polluted air and biomass burning smoke

D. Rose et al.

cloud types: Application to droplet concentration parameterization of aerosol conditions, J. Geophys. Rev., 111, D15204, doi:10.1029/2005JD006561, 2006.

Shao, M., Tang, X., Zhang, Y., and Li, W.: City clusters in China: air and surface water pollution, Front. Ecol. Environ., 4, 353–361, 2006.

Streets, D. G., Tsai, N. Y., Akimoto, H., and Oka, K.: Sulfur dioxide emissions in Asia in the period 1985–1997, Atmos. Environ., 34, 4413–4424, 2000.

Streets, D. G., Yu, C., Wu, Y., Chin, M., Zhao, Z., Hayasaka, T., and Shi, G.: Aerosol trends over China, 1980–2000, Atmos. Res., 88, 174–182, 2008.

Wang, X., Carmichael, G., Chen, D., Tang, Y., and Wang, T.: Impacts of different emission sources on air quality during March 2001 in the Pearl River Delta (PRD) region, Atmos. Environ., 39, 5227–5241, 2005.

Wehner, B., Berghof, M., Achtert, P., Nowak, A., Wiedensohler, A., Garland, R. M., Pöschl, U., Cheng, Y. F., Hu, M., Zhang, Y. H., and Zhu, T.: Mixing state of non volatile particle fractions and comparison with absorption measurements in the polluted Beijing-region, J. Geophys. Res.-Atmos., submitted, 2008.

Wendisch, M., Hellmuth, O., Ansmann, A., Heintzenberg, J., Engelmann, R., Althausen, D., Eichler, H., Müller, D., Hu, M., Zhang, Y., and Mao, J.: Radiative and dynamic effects of absorbing aerosol particles over the Pearl River Delta, China, Atmos. Environ., 42, 6405–6416, 2008.

Wiedensohler, A., Cheng, Y. F., Nowak, A., Wehner, B., Achtert, P., Berghof, M., Birmili, W., Wu, Z. J., Hu, M., Zhu, T., Takegawa, N., Kita, K., Kondo, Y., Lou, S. R., Hofzumahaus, A., Holland, F., Wahner, A., Gunthe, S. S., Rose, D., and Pöschl, U.: Rapid Aerosol Particle Growth and Increase of Cloud Condensation Nucleus (CCN) Activity by Secondary Aerosol Formation: a Case Study for Regional Air Pollution in North Eastern China, J. Geophys. Res.-Atmosp., submitted, 2008.

Xu, Q.: Abrupt change of the mid-summer climate in central east China by the influence of atmospheric pollution, Atmos. Environ., 35, 5029–5040, 2001.

Yum, S. S., Hudson, J. G., Song, K. Y., and Choi, B. C.: Springtime cloud condensation nuclei concentrations on the west coast of Korea, Geophys. Res. Lett., 32, L09814, doi:10.1029/2005GL022641, 2005.

Yum, S. S., Roberts, G., Kim, J. H., Song, K. Y., and Kim, D. Y.: Submicron aerosol size distributions and cloud condensation nuclei concentrations measured at Gosan, Korea, during the Atmospheric brown clouds East Asian Regional Experiment 2005, J. Geophys. Res., 112,

CCN in polluted air and biomass burning smoke

D. Rose et al.

- Title Page
- Abstract | Introduction
- Conclusions | References
- Tables | Figures
- |◄ | ►|
- ◄ | ►
- Back | Close
- Full Screen / Esc
- Printer-friendly Version
- Interactive Discussion

D22S32, doi:10.1029/2006JD008212, 2007.

Zhang, Y. H., Hu, M., Zhong, L. J., Wiedensohler, A., Liu, S. C., Andreae, M. O., Wang, W., and Fan, S. J.: Regional Integrated Experiments on Air Quality over Pearl River Delta 2004 (PRIDE-PRD2004): Overview, Atmos. Environ., 42, 6157–6173, doi:10.1016/j.atmosenv.2008.03.025, 2008.

Zhang, Y. L., Qin, B. Q., and Chen, W. M.: Analysis of 40 year records of solar radiation data in Shanghai, Nanjing and Hangzhou in Eastern China, Theor. Appl. Climatol., 78, 217–227, 2004.

Zhao, C., Tie, X., and Lin, Y.: A possible positive feedback of reduction of precipitation and increase in aerosols over eastern central China, Geophys. Res. Lett., 33, L11814, doi:10.1029/2006GL025959, 2006.

CCN in polluted air and biomass burning smoke

D. Rose et al.

Title Page

Abstract | Introduction

Conclusions | References

Tables | Figures

|◀ | ▶|

◀ | ▶

Back | Close

Full Screen / Esc

Printer-friendly Version

Interactive Discussion

**CCN in polluted air
and biomass burning
smoke**

D. Rose et al.

Table 1. Characteristic parameters from the 5 calibration experiments performed during the campaign (arithmetic mean±standard deviation). The last column shows the maximum relative deviation of individual calibration data points from the average calibration line (S vs. ΔT), indicating maximum relative uncertainties in S.

ΔT [K]	D_a [nm]	S [%]	$\Delta S/S$ [%]
1.99±0.02	158.8±5.2	0.072±0.004	6.9
4.46±0.01	66.7±1.9	0.28±0.01	5.8
10.70±0.02	35.3±1.0	0.75±0.04	5.9
14.44±0.01	28.2±0.8	1.06±0.05	6.7
16.95±0.02	24.9±0.7	1.29±0.06	6.7

Table 2. Characteristic average CCN parameters (arithmetic mean values±standard deviation) for the entire campaign, for the biomass burning event (BBE, 23–26 July) and for the campaign excluding the BBE: midpoint activation diameters (D_a,D_{50},D_t), maximum activated fractions (MAF$_f$, MAF$_m$), CDF standard deviations (σ_a, σ_t), heterogeneity parameters (σ_a/D_a, σ_t/D_t), hygroscopicity parameters (κ_a,κ_{50}, κ_t), number concentrations of total aerosol particles (3–900 nm, $N_{CN,tot}$) and of cloud condensation nuclei ($N_{CCN,S}$), and ratio of $N_{CN,tot}$ to $N_{CCN,S}$ as defined in Sect. 2.2.4. n_{es} and n_{sd} are the numbers of averaged CCN efficiency spectra and size distributions, respectively.

S [%]	D_a [nm]	D_{50} [nm]	D_t [nm]	MAF$_f$	MAF$_m$	σ_a [nm]	σ_t [nm]	σ_a/D_a	σ_t/D_t
Entire campaign									
0.07	186.9±11.4	199.5±29.8	206.4±18.3	0.74±0.13	0.74±0.14	17.3±10.3	48.2±23.3	0.09±0.06	0.23±0.10
0.27	81.3±8.8	83.0±9.9	85.2±12.8	0.89±0.09	0.93±0.10	9.4±6.9	14.0±9.6	0.11±0.07	0.16±0.10
0.47	59.5±6.9	60.0±7.3	61.2±13.1	0.95±0.07	0.98±0.08	6.0±4.7	6.9±5.7	0.10±0.06	0.11±0.07
0.67	49.1±5.9	49.6±6.1	50.1±6.4	0.96±0.07	0.99±0.08	5.5±4.2	6.5±4.9	0.11±0.07	0.12±0.08
0.87	41.2±4.6	41.4±4.6	41.6±5.0	0.98±0.07	1.00±0.08	4.5±3.1	4.8±3.2	0.11±0.06	0.11±0.06
1.27	32.0±3.5	32.2±3.5	32.4±3.6	0.97±0.05	1.02±0.05	4.6±2.6	5.3±2.8	0.14±0.07	0.16±0.07
BBE									
0.07	202.4±9.4	216.4±45.8	216.5±16.6	0.75±0.10	0.75±0.11	15.9±8.8	36.3±16.2	0.08±0.04	0.17±0.07
0.27	94.3±11.8	97.4±12.8	99.0±12.5	0.88±0.08	0.92±0.10	18.6±8.4	23.7±8.0	0.19±0.08	0.24±0.07
0.47	69.0±9.0	70.2±9.6	71.6±10.1	0.92±0.05	0.96±0.05	11.7±6.3	14.0±7.2	0.16±0.07	0.19±0.08
0.67	60.0±6.9	61.4±7.0	62.6±7.5	0.92±0.05	0.94±0.06	12.5±4.1	14.9±5.5	0.20±0.05	0.23±0.07
0.87	47.2±5.6	47.8±5.9	48.6±6.8	0.94±0.04	0.97±0.05	7.4±3.3	8.6±4.4	0.15±0.06	0.17±0.07
1.27	35.1±4.2	35.6±4.2	36.2±3.8	0.92±0.07	0.99±0.03	6.5±3.3	8.4±2.5	0.18±0.08	0.23±0.06
Entire campaign excluding BBE									
0.07	184.6±9.8	197.0±25.9	204.9±18.1	0.73±0.13	0.74±0.14	17.5±10.5	50.0±23.7	0.10±0.06	0.24±0.10
0.27	79.5±6.6	81.1±7.6	83.4±11.6	0.89±0.09	0.93±0.10	8.2±5.6	12.7±9.0	0.10±0.06	0.15±0.09
0.47	58.3±5.5	58.7±5.9	59.8±12.8	0.95±0.07	0.98±0.08	5.2±3.9	6.0±4.8	0.09±0.05	0.10±0.06
0.67	48.2±4.7	48.6±4.8	49.0±5.1	0.96±0.07	0.99±0.08	4.9±3.6	5.7±4.1	0.10±0.06	0.11±0.07
0.87	40.5±3.9	40.6±3.8	40.8±4.0	0.99±0.07	1.01±0.08	4.2±2.9	4.4±2.7	0.10±0.06	0.10±0.06
1.27	31.3±2.9	31.5±2.9	31.6±3.0	0.98±0.04	1.02±0.06	4.2±2.3	4.6±2.4	0.13±0.06	0.14±0.07

Table 2. Continued.

S [%]	κ_a	κ_{50}	κ_t	$N_{CN,tot}$ [cm^{-3}]	$N_{CCN,S}$ [cm^{-3}]	$N_{CCN,S}/N_{CN,tot}$	n_{es}	n_{sd}
Entire campaign								
0.07	0.46±0.09	0.40±0.09	0.35±0.09		1099±795	0.07±0.05	387	301
0.27	0.37±0.10	0.35±0.10	0.33±0.11		6640±3975	0.36±0.16	381	287
0.47	0.31±0.09	0.31±0.09	0.30±0.10		9553±5117	0.53±0.19	413	321
0.67	0.28±0.08	0.27±0.09	0.26±0.09		10 872±6066	0.59±0.19	275	210
0.87	0.27±0.08	0.27±0.08	0.27±0.08		12 884±6440	0.70±0.18	400	312
1.27	0.27±0.08	0.27±0.08	0.27±0.08		15 819±5756	0.85±0.10	112	86
all	0.34±0.11	0.32±0.10	0.30±0.10	18 216±8022			1968	1517
BBE								
0.07	0.36±0.05	0.32±0.08	0.30±0.06		1986±1210	0.14±0.06	49	48
0.27	0.24±0.09	0.22±0.09	0.21±0.08		7233±4008	0.46±0.16	45	44
0.47	0.21±0.08	0.20±0.08	0.19±0.08		8823±4470	0.59±0.16	47	46
0.67	0.15±0.06	0.14±0.05	0.13±0.06		8597±5774	0.54±0.12	22	20
0.87	0.19±0.06	0.18±0.06	0.17±0.07		11 119±5863	0.72±0.15	43	41
1.27	0.21±0.07	0.20±0.07	0.19±0.06		13 563±4247	0.84±0.08	19	19
all	0.24±0.10	0.22±0.09	0.21±0.09	15 273±6562			225	218
Entire campaign excluding BBE								
0.07	0.48±0.08	0.41±0.09	0.36±0.09		925±529	0.05±0.03	338	253
0.27	0.39±0.09	0.37±0.09	0.35±0.10		6531±3968	0.35±0.15	336	243
0.47	0.33±0.08	0.32±0.08	0.32±0.09		9675±5216	0.52±0.19	366	275
0.67	0.29±0.08	0.28±0.08	0.27±0.08		11 111±6062	0.60±0.20	253	190
0.87	0.29±0.08	0.28±0.08	0.28±0.08		13 151±6493	0.70±0.19	357	271
1.27	0.29±0.07	0.28±0.07	0.28±0.07		16 460±5989	0.85±0.10	93	67
all	0.35±0.11	0.33±0.10	0.32±0.10	18 710±8140			1743	1299

Table 3. Characteristic deviations between measured CCN number concentrations $N_{\text{CCN,S}}$ and CCN number concentrations predicted by different model approaches ($N_{\text{CCN,S,p}}$): arithmetic mean values of the relative bias ($\Delta_b N_{\text{CCN,S}}=(N_{\text{CCN,S,p}}-N_{\text{CCN,S}})/N_{\text{CCN,S}}$) and of the total relative deviation ($\Delta_d N_{\text{CCN,S}}=|N_{\text{CCN,S,p}}-N_{\text{CCN,S}}|/N_{\text{CCN,S}}$, including systematic and statistical errors). CPL is the classical power law and MPL the modified power law approach, respectively. n_{sd} is the number of data points.

S [%]	CPL		MPL		κ_t individual		κ_a individual		κ_{50} individual		$\kappa=0.3$		$\kappa_a=0.34$		$\kappa_{50}=0.32$		n_{sd}
	bias [%]	dev. [%]	bias [%]	dev. [%]	bias [%]	dev. [%]	bias [%]	dev. [%]	bias [%]	dev. [%]	bias [%]	dev. [%]	bias [%]	dev. [%]	bias [%]	dev. [%]	
0.07	268.7	271.5	29.1	59.0	10.1	12.1	41.4	41.4	23.8	27.0	1.5	19.0	15.9	23.8	8.7	20.8	301
0.27	46.7	82.5	22.7	40.3	6.5	7.1	12.6	12.9	9.6	10.0	5.3	15.2	12.2	17.7	8.8	16.3	287
0.47	38.1	74.9	15.3	27.3	4.3	5.7	6.4	7.1	5.4	6.0	7.9	12.2	12.3	14.5	10.2	13.3	321
0.67	55.0	84.6	13.5	22.3	3.2	4.2	4.9	5.6	4.2	4.7	10.6	13.1	14.1	15.6	12.4	14.3	210
0.87	42.2	70.5	7.7	13.5	2.7	3.4	3.4	3.8	3.2	3.5	7.4	8.8	9.7	10.5	8.6	9.7	312
1.27	24.4	45.2	0.9	3.8	4.1	4.2	4.5	4.6	4.3	4.5	5.4	5.8	7.1	7.1	5.9	6.1	86
all	87.9	114.1	16.8	31.2	5.4	6.5	13.6	14.0	9.1	10.2	6.2	13.2	12.4	15.9	9.3	14.4	1517

Table 4. Fit parameter Q and q of the fit functions $N_{CCN,S} = N_{CN,30} \cdot \left(S/(1\%) \right)^{Q}$ and $N_{CCN,S} = N_{CN,30} \cdot s^{-q}$, respectively. The correlation coefficient R^2 is the same for both fits. n_{sd} is the number of data points.

S [%]	s	Q	q	R^2	n_{sd}
0.07	1.0007	1.08	3912	0.09	301
0.27	1.0027	0.65	316.1	0.61	287
0.47	1.0047	0.61	98.13	0.80	321
0.67	1.0067	0.79	47.37	0.88	210
0.87	1.0087	1.28	20.52	0.94	312
1.27	1.0127	−0.35	6.54	0.98	86
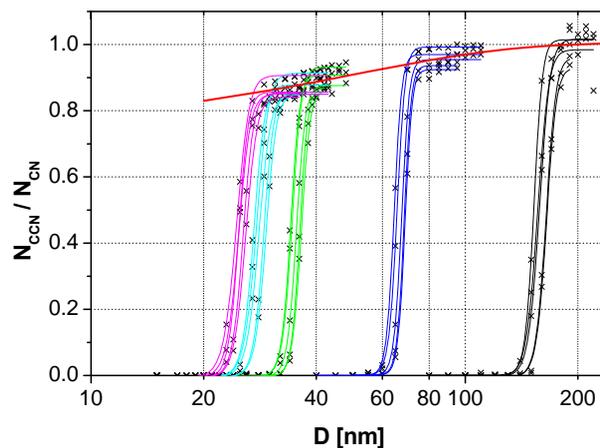
Fig. 1. CCN efficiency spectra obtained from 5 calibration experiments with ammonium sulfate aerosol performed during the campaign (data points and CDF fits). The red line is the asymptotic function that was used to correct for different counting efficiencies of the CPC and the CCNC (f_{corr}).
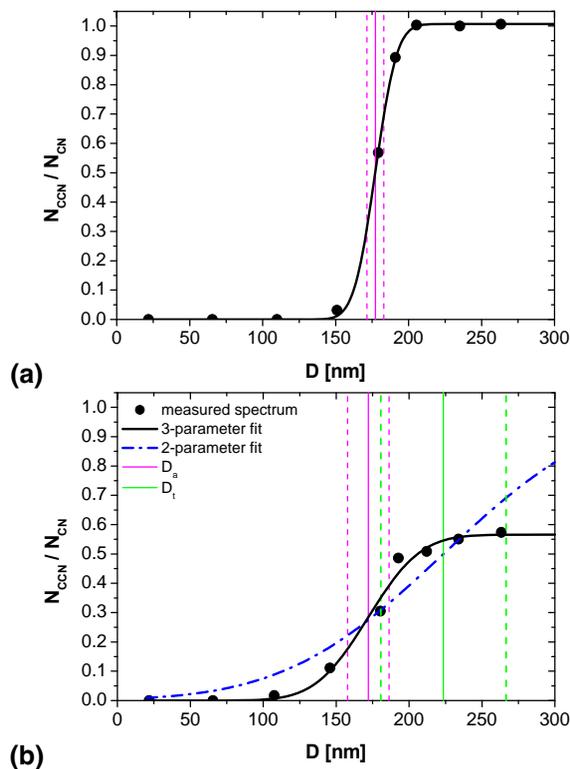
Fig. 2. Exemplary CCN efficiency spectra **(a)** with "ideal" shape (12 July 2006, 18:55–19:06), and **(b)** with low maximum fraction of activated particles (9 July 2006, 03:23–03:34): measurement data points (corrected according to Sect. 2.2.3; black dots); 3-parameter CDF fit (black solid line) with fit parameters D_a (pink line), and σ_a (distance between pink dashed lines); 2-parameter CDF fit (blue dash-dotted line) with fit parameters D_t (green line) and σ_t (distance between green dashed lines).

17380
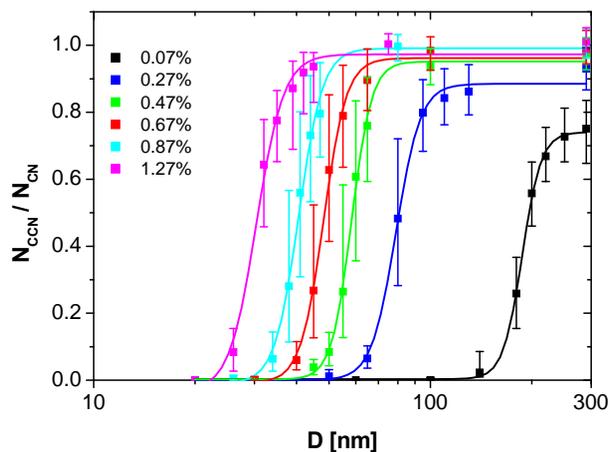
Fig. 3. CCN efficiency spectra at S=0.07%–1.27% averaged over the entire campaign. The data points are median values calculated from the CDF fits to all measured spectra at the particle diameters initially selected with the DMA (20–290 nm). The error bars extend from the lower to the upper quartile, and the lines are 3-parameter CDF fits to the data points (Sect. 2.2.4).
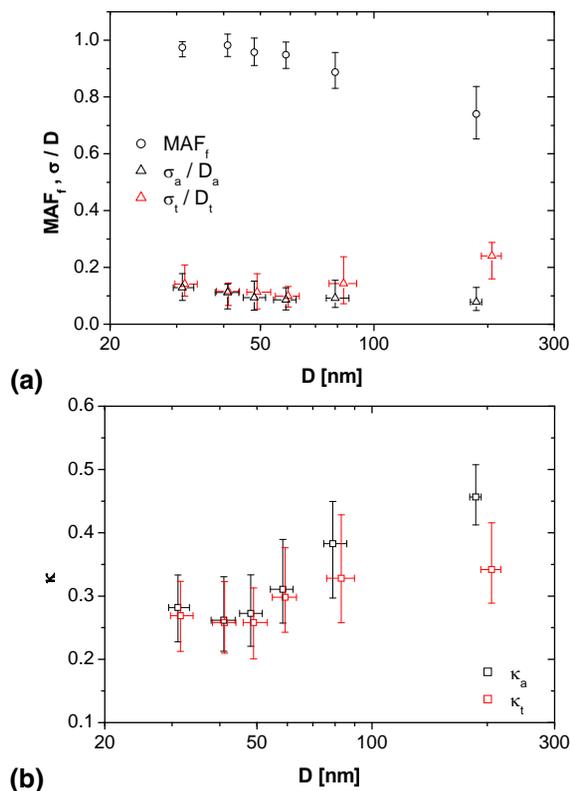
Fig. 4. Characteristic parameters derived from the CCN efficiency spectra averaged over the entire campaign: **(a)** maximum activated fractions (MAF_f) and heterogeneity parameters (σ_a/D_a, σ_t/D_t); **(b)** hygroscopicity parameters (κ_a, κ_t) plotted against the midpoint activation diameter (D_a or D_t, respectively). The data points are median values corresponding to a given level of supersaturation, and the error bars extend to lower and upper quartiles.
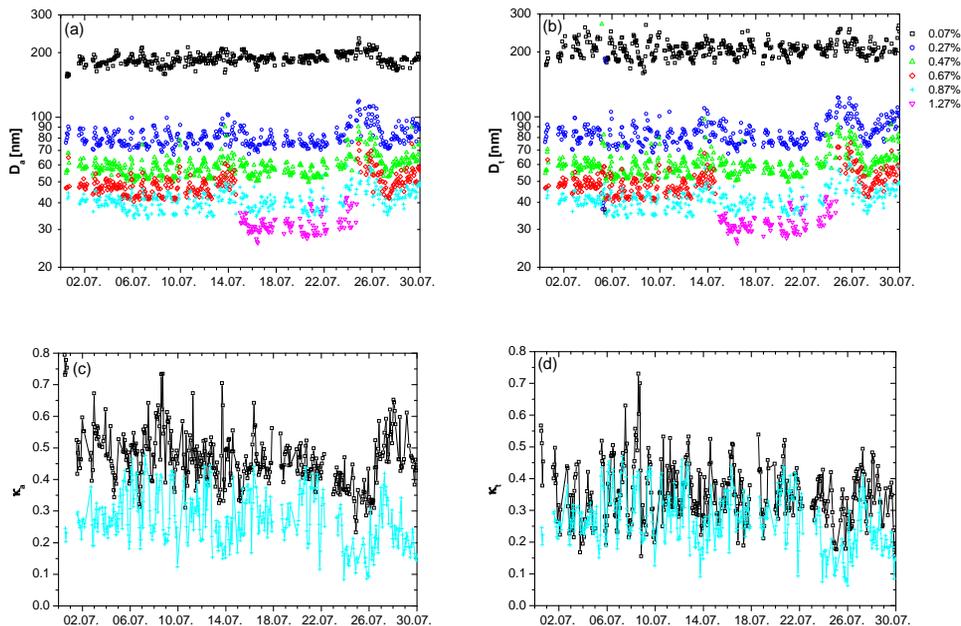
Fig. 5. Time series of the characteristic parameters derived from the CCN efficiency spectra measured at different supersaturations plotted against the date in July 2006.
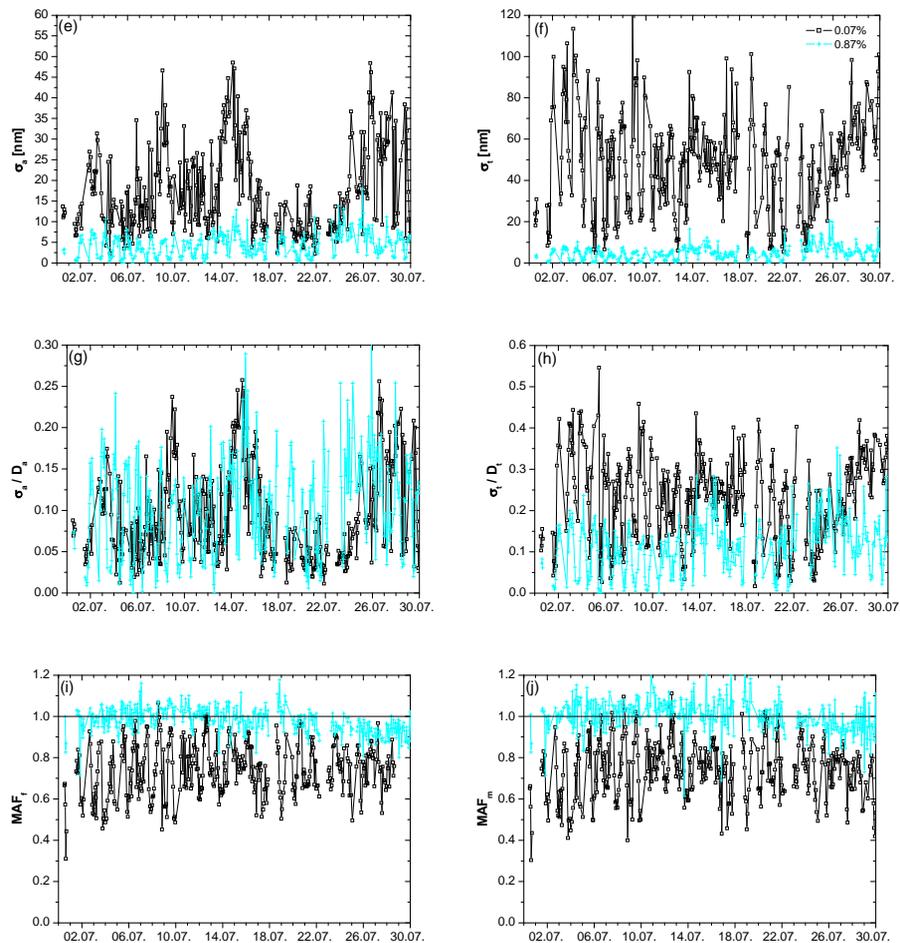
Fig. 5. Continued.

CCN in polluted air and biomass burning smoke

D. Rose et al.
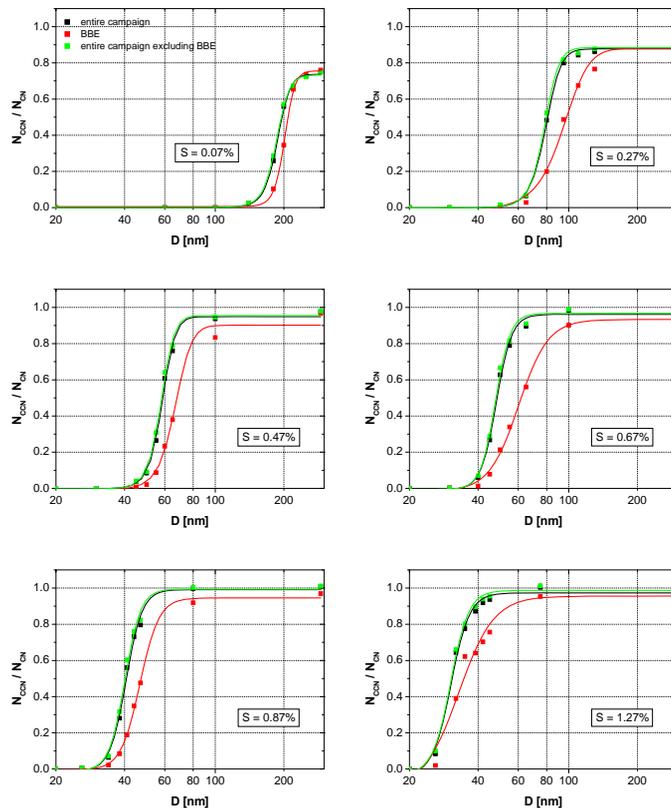
Fig. 6. CCN efficiency spectra for different supersaturation levels and periods: entire campaign (black), biomass burning event (BBE, red), and entire campaign excluding the BBE (green). The data points are median values, and solid lines are CDF fits through them.

(a)

(b)
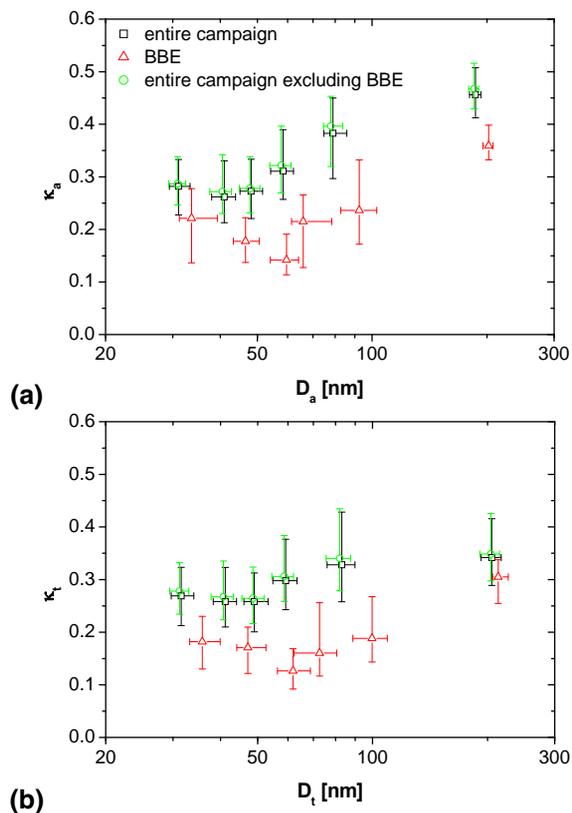
Fig. 7. Hygroscopicity parameters **(a)** for the CCN-active particles (κ_a) and **(b)** for the total aerosol (κ_t) averaged over different periods: the entire campaign, the biomass burning event and the campaign excluding the biomass burning event. The data points are median values corresponding to a given level of supersaturation, and the error bars extend to lower and upper quartiles.

(a)

(b)
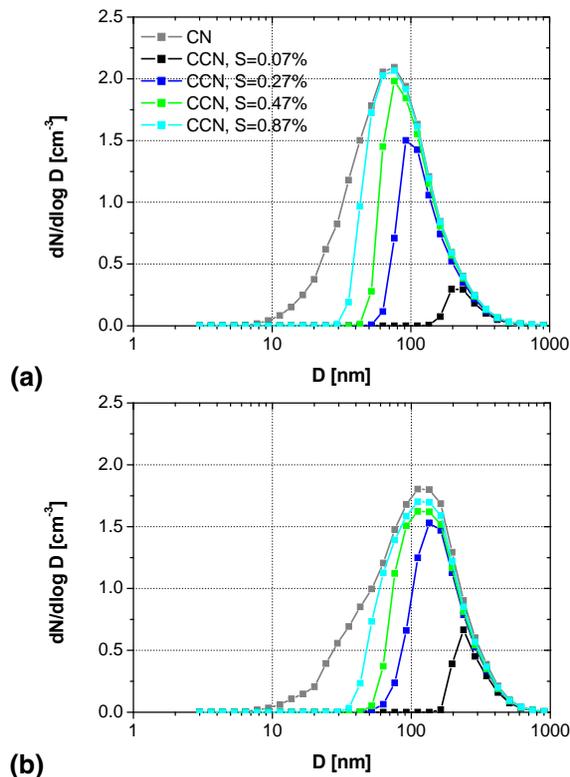
Fig. 8. Number size distributions of total aerosol particles (CN) and cloud condensation nuclei (CCN) averaged over **(a)** the entire campaign and **(b)** the biomass burning event. The CCN size distributions were calculated by multiplying the median CN size distribution with the median CCN efficiency spectra from Fig. 3. For clarity and to avoid potential biases due to different averaging times, CCN size distributions are displayed only for the supersaturation levels covered throughout the campaign.
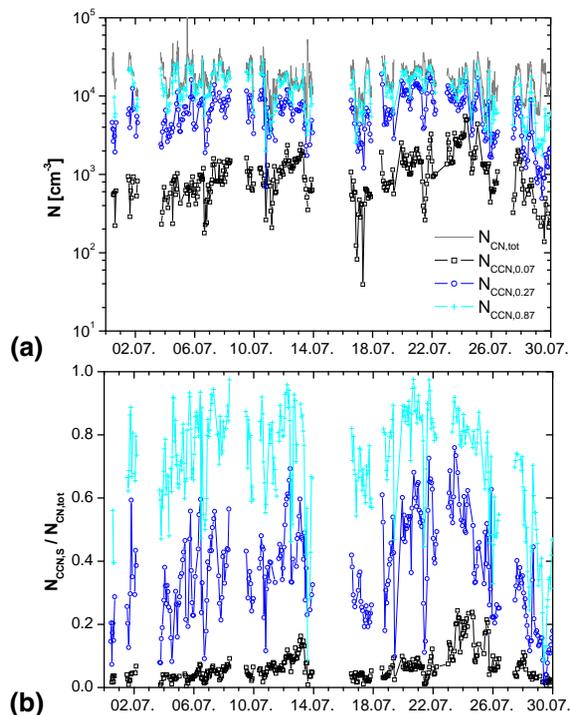
Fig. 9. Time series of **(a)** the number concentration of total aerosol particles ($N_{CN,tot}$) and cloud condensation nuclei ($N_{CCN,S}$) and **(b)** the integral CCN efficiencies ($N_{CCN,S}/N_{CN,tot}$) at different supersaturation levels (S=0.07%, 0.27%, and 0.87%) plotted against the date in July 2006.
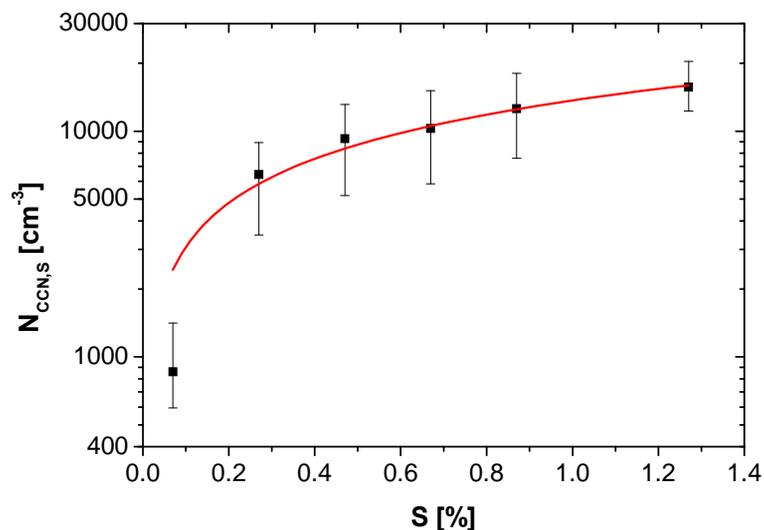
Fig. 10. CCN number concentrations ($N_{CCN,S}$) averaged over the entire campaign and plotted against water vapor supersaturation (S). The data points are median values, and error bars extend to lower and upper quartiles. The red line is a classical power law fit of the function $N_{CCN,S}=N_{CCN,1}\cdot(S/(1\%))^k$ with the best fit parameters $N_{CCN,1}=13\,699\,\mathrm{cm}^{-3}$ and $k=0.65$ ($R^2=0.97$, $n=6$).
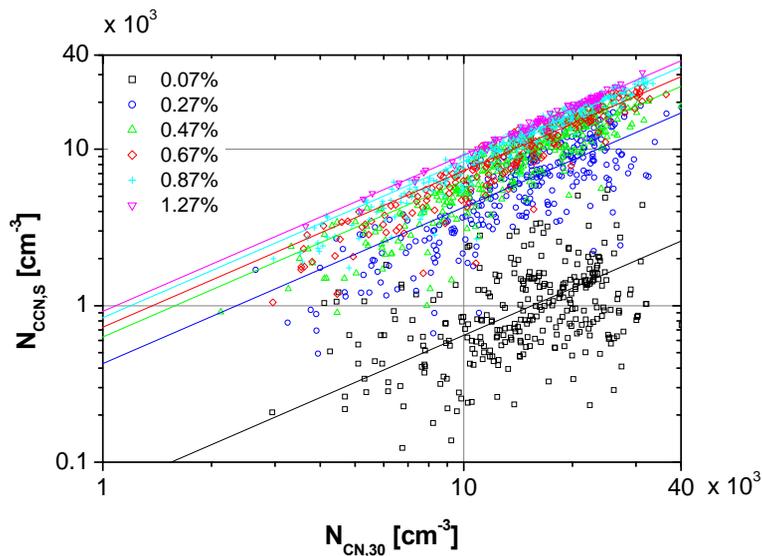
Fig. 11. CCN number concentrations ($N_{CCN,S}$) measured at different supersaturation levels plotted against the number concentration of aerosol particles with $D>30$ nm ($N_{CN,30}$). The lines are modified power law fits of the function $N_{CCN,S}=N_{CN,30} \cdot s^{-q}$ with the parameter q as given in Table 4.
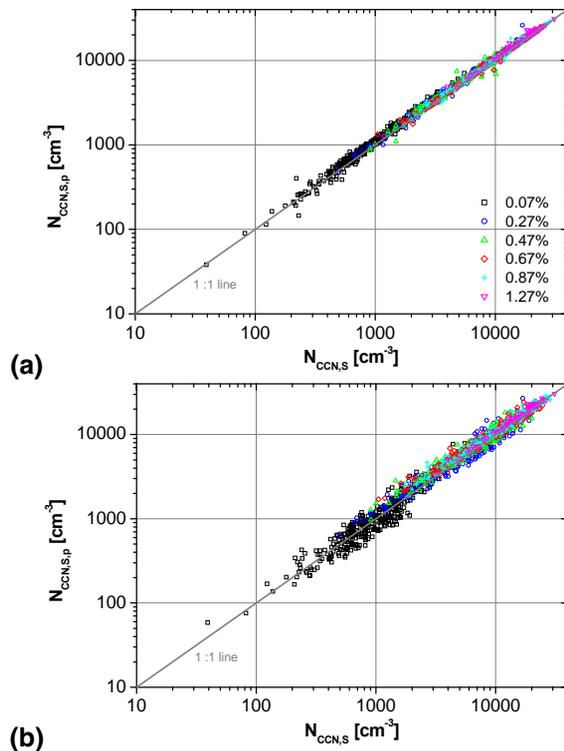
Fig. 12. Predicted CCN number concentrations ($N_{\mathrm{CCN,S,p}}$) based on the κ-Köhler model approach **(a)** with variable values of κ_t as derived from individual CCN efficiency spectra and **(b)** with a constant average value of $\kappa = 0.3$ plotted against the measured CCN number concentrations ($N_{\mathrm{CCN,S}}$).
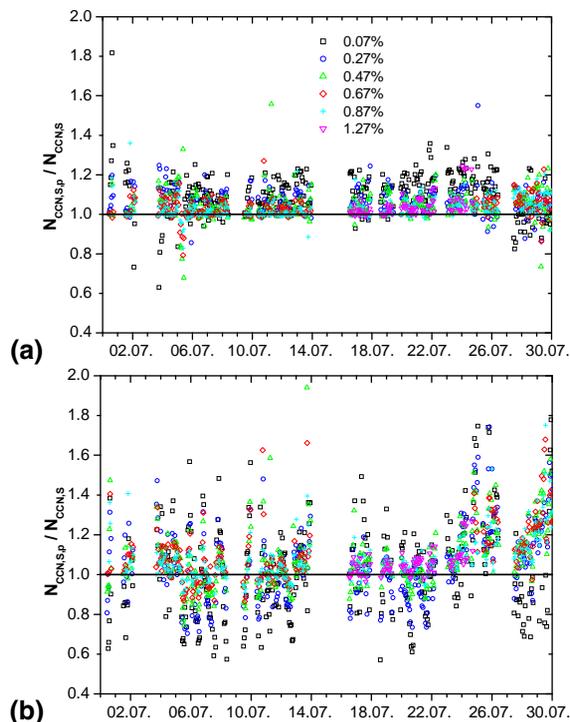
Fig. 13. Time series of the ratio of predicted and measured CCN number concentrations ($N_{CCN,S,p}/N_{CCN,S}$) based on the κ-Köhler model approach **(a)** with κ_t as derived from the individual CCN efficiency spectra and **(b)** with a constant average value of $\kappa=0.3$ plotted against the date in July 2006.